Supplementary Information for

Drying Mediated Orientation and Assembly Structure of Amphiphilic Janus Particles

Kyle Miller,[a†] Ayuna Tsyrenova,[a] Stephen M. Anthony,[b] Shiyi Qin,[c] Xin Yong*[c] and Shan Jiang*[ad]

[a] *Department of Materials Science and Engineering, Iowa State University of Science and Technology, Ames, IA 50011, USA. E-mail: sjiang1@iastate.edu*

[b] *Department of Bioenergy and Defense Technology, Sandia National Laboratories, Albuquerque, NM, USA*

[c] *Department of Mechanical Engineering and Institute for Materials Research, Binghamton University, Binghamton, NY, 13902, USA. E-mail: xyong@binghamton.edu*

[d] *Division of Materials Science & Engineering, Ames National Laboratory, Ames, IA 50011, USA*

1. Janus particle synthesis and drying experiment

Janus particles were fabricated following a protocol developed previously.[1] Thin layers of Cr (adhesion layer) and Au (top layer) were deposited sequentially onto a monolayer of 3 μm silica particles using e-beam evaporation (Temescal BJD-1800). Thiol molecules are then used to render Au surface with different chemical properties. ODT (1-octadecanethiol) and DDT (1-Dodecanethiol) are used to render Au surface hydrophobic and obtain amphiphilic Janus particles (JP-ODT and JP-DDT), while MHA (16-Mercaptohexadecanoic acid) is used to give the Au surface a negative charge (JP-MHA). Thiol chemicals were obtained from Sigma Aldrich, 200 proof ethanol from Decon Labs. To obtain Janus particles of different Janus balance, coated Janus particles were etched by aqua regia (both HCl and HNO_3 from Fisher) diluted with varying amounts of water. After a set time, particles were removed, rinsed, and rendered amphiphilic with thiol. Control particles (JP-SiO_2), which are optically Janus however chemically homogeneous, were obtained by depositing another layer of silica onto the Au coated particle monolayer instead of the thiol treatment.

For the drying experiment, we only used hydrophilic substrate cleaned by O_2 plasma. Glass slides were cleaned in a base bath and silicon wafers cleaned with ethanol, then substrates were

rinsed thoroughly with deionized water (resistivity 18.3 MΩ·cm; Barnstead EASYpure LF), and treated with oxygen plasma for at least 10 min (Harrick Plasma PDC001). The substrates were used directly after cleaning for the drying experiment. In a typical experiment, a droplet of the aqueous particle solution was applied to a clean substrate at room temperature and allowed to dry.

The particles were imaged via optical microscopy on a Leica DMi8, while SEM images were taken on either a FEI Inspect F50 or FEI Quanta 250 (which produce roughly equivalent images). Both backscattering and secondary scattering images were taken and fed into an algorithm (see below) developed to extract orientation of Janus particles. For observation, we focus on the monolayer of particles formed inside the boundary of the thick coffee ring pattern.

2. Hemispherical Janus Particle Orientation Calculations

a. Janus Particle Defininition

Janus particles are particles with two faces; in this case, one portion of the Janus particle is coated and the other uncoated. In this work, we will be restricting our analysis to spherical Janus particles with one hemisphere coated and one uncoated. If the particle is oriented directly towards the observer, it will appear radially symmetric, and the center of the coated region would appear at spherical coordinates $(r,\theta,\varphi) = (r,0,0)$, where r is the radius of the particle. As such, the orientation of the Janus particle can be defined by the position of the center of the coated side using the variables $\theta \in 0,\pi$ and $\varphi \in 0,2\pi$, where θ is the polar angle and φ is the azimuthal angle. Therefore, hemispherically coated Janus particles can be described using the coordinates $P(r,\theta,\varphi)$, where for simplicity we will define the center of the sphere as the origin.

b. Boundary Line Determination

For a hemispherically coated Janus particle whose coated face is oriented directly at the observer, $P(r,0,0)$, the cartesian coordinates of the boundary line separating the coated from the uncoated side will be:

$$z = 0$$
$$2\ 2\ 2\ x + y = r \qquad (1)$$

Expressing this in terms of x, y, and z, where $y_0 = [-r,r]$:

$$\begin{bmatrix} x \\ y \\ z \end{bmatrix} = \begin{bmatrix} \pm\sqrt{r^2 - y_0^2} \\ y_0 \\ 0 \end{bmatrix} \tag{2}$$

Of course, this is limited to particles oriented with the coated side directly facing the observer, $P(r,0,0)$. Converting to particles with arbitrary polar angles, $P(r,\theta,0)$, requires roatating clockwise around the y-axis. The necessary rotation matrix is given by:

$$R_y(\theta) = \begin{bmatrix} \cos\theta & 0 & \sin\theta \\ 0 & 1 & 0 \\ -\sin\theta & 0 & \cos\theta \end{bmatrix} \tag{3}$$

Applying the rotation matrix R_y to the coordinates of the boundary line for $P(r,0,0)$ yields the Cartesian coordinates of the boundary line for $P(r,\theta,0)$:

$$\begin{bmatrix} x \\ y \\ z \end{bmatrix} = \begin{bmatrix} \pm\cos\theta\sqrt{r^2 - y_0^2} \\ y_0 \\ \mp\sin\theta\sqrt{r^2 - y_0^2} \end{bmatrix} \tag{4}$$

Converting to particles with arbitrary azimuthal angles, $P(r,\theta,\varphi)$, requires roatating counterclockwise around the z-axis. The necessary rotation matrix is given by:

$$R_z(\phi) = \begin{bmatrix} \cos\phi & \sin\phi & 0 \\ -\sin\phi & \cos\phi & 0 \\ 0 & 0 & 1 \end{bmatrix} \tag{5}$$

Applying the rotation matrix R_z to the coordinates of the boundary line for $P(r,\theta,0)$ yields the Cartesian coordinates of the boundary line for $P(r,\theta,\varphi)$:

$$\begin{bmatrix} x \\ y \\ z \end{bmatrix} = \begin{bmatrix} \pm\cos\phi\cos\theta\sqrt{r^2 - y_0^2} + y_0\sin\phi \\ \mp\sin\phi\cos\theta\sqrt{r^2 - y_0^2} + y_0\cos\phi \\ \mp\sin\theta\sqrt{r^2 - y_0^2} \end{bmatrix} \tag{6}$$

c. Observable Boundary

Of course, Equation 7 provides the Cartesian coordinates of the entire boundary separating the coated hemisphere from the uncoated hemisphere. However, only the portion of the boundary

line where $z \geq 0$ will be directly visible to ther observer. Barring the cases where the coated hemisphere is oriented directly at ($\theta = 0$) or directly away ($\theta = \pi$) from the observer, the 2-dimensional projection of the coated region will be bounded on one side by the visible boundary line and on the other side by the edge of the sphere. These two curves can be seen to intersect at the points on the boundary line where $z = 0$. Neglecting the trivial cases where $\theta = 0$ or $\theta = \pi$, then $\sin\theta \geq 0$. Therefore, it can be immediately seen that the visible portion of the boundary line is given by

$$\begin{bmatrix} x \\ y \\ z \end{bmatrix} = \begin{bmatrix} -\cos\phi\cos\theta\sqrt{r^2 - y_0^2} + y_0\sin\phi \\ \sin\phi\cos\theta\sqrt{r^2 - y_0^2} + y_0\cos\phi \\ \sin\theta\sqrt{r^2 - y_0^2} \end{bmatrix} \tag{7}$$

d. Fractional Area

The 2-dimensional image of the hemispherically coated Janus particle is converted to a binary image which is true wherever the coated portion of the Janus particle is observable and false elsewhere. If the centroid of the coated region is calculated from this binary image, the distance $d_{centroid}$ between the centroid and the center of the sphere can be used to determine the polar angle θ. The azimuthal angle φ has no effect upon $d_{centroid}$.

Therefore, for simplicity it is easiest to perform the calculation assuming that $\varphi = 0$, in which case the two boundary curves in 2D Cartesian coordinates are specified by

$$\begin{bmatrix} x \\ y \end{bmatrix}_{boundary} = \begin{bmatrix} -\cos\theta\sqrt{r^2 - y_0^2} \\ y_0 \end{bmatrix} \tag{8}$$

and

$$\begin{bmatrix} x \\ y \end{bmatrix}_{edge} = \begin{bmatrix} \sqrt{r^2 - y_0^2} \\ y_0 \end{bmatrix} \tag{9}$$

The area A of the 2D projection of the coated region can be found by integrating:

$$\begin{aligned} A &= \int_{-r}^{r} \sqrt{r^2 - y_0^2} + \cos\theta\sqrt{r^2 - y_0^2}\,dy \\ &= \pi r^2 \cos^2\frac{\theta}{2} \\ &= \pi r^2 \frac{\cos\theta + 1}{2} \end{aligned} \tag{10}$$

As such, the fraction of the 2D projection occupied by the coated region can trivially be found by dividing by the area of the circle, yielding:

$$\begin{aligned} A &= \frac{\cos\theta + 1}{2} \\ 2A &= \cos\theta + 1 \\ 2A - 1 &= \cos\theta \\ \theta &= \cos^{-1}(2A - 1) \end{aligned} \tag{11}$$

e. Centroid

Since the coated region is clearly symmetric across the x-axis when $\varphi = 0$, the centroid must lie along the x-axis. Therefore, there is no need to compute the y-coordinate of the centroid, as $\bar{y} = 0$. The x-coordinate of the centroid can be computed by integrating

$$\begin{aligned} \bar{x} &= \frac{1}{2A}\int_{-r}^{r} \left(r^2 - y_0^2\right) - \cos^2\theta\left(r^2 - y_0^2\right) dy \\ &= \frac{1}{2A}\int_{-r}^{r} \left(1 - \cos^2\theta\right)\left(r^2 - y_0^2\right) dy \\ &= \frac{1}{2A}\int_{-r}^{r} \sin^2\theta\left(r^2 - y_0^2\right) dy \\ &= \frac{1}{2A}\frac{4r^3\sin^2\theta}{3} \\ &= \frac{1}{A}\frac{2r^3\sin^2\theta}{3} \\ &= \frac{1}{\pi r^2\cos^2\frac{\theta}{2}}\frac{2r^3\sin^2\theta}{3} \\ &= \frac{4r}{3\pi}\frac{\sin^2\theta}{2\cos^2\frac{\theta}{2}} \\ &= \frac{4r}{3\pi}(1 - \cos\theta \end{aligned} \qquad) \tag{12}$$

Solving for θ yields:

$$\begin{aligned} \bar{x} &= \frac{4r}{3\pi} - \frac{4r}{3\pi}\cos\theta \\ \frac{4r}{3\pi}\cos\theta &= \frac{4r}{3\pi} - \bar{x} \\ \cos\theta &= 1 - \frac{3\pi}{4r}\bar{x} \\ \theta &= \cos^{-1}\left(1 - \frac{3\pi}{4r}\bar{x}\right) \end{aligned} \tag{13}$$

f. Program

The location and orientation of each of the Janus particles is determined using custom code developed in Matlab R2017a (Mathworks, Natick, MA). Two SEM images are employed, one optimized for detection of the particle edges and the other optimized for detection of the coating. To reduce the effect of pixelation, the images are first interpolated to double the resolution. The location of the particles in each image is then determined using Matlab's imfindcircles routine, which employs the Circular Hough Transform. In general, most particles are detected in both images, although particles where the uncoated side is oriented towards the observer may not be detected in the SEM image optimized for sensitivity to the coating. Therefore, the locations of the particles in the SEM image optimized for particle detections are used throughout the rest of the analysis.

In contrast, the SEM image optimized for detecting the coating is more useful when determining the orientation. Since the locations were computed using a different image, first it is necessary to account for any possible rotation or translation between the images. Since any shifts in alignment are minor, the corresponding particles in the two images are easily determined by solving the linear assignment problem to determine matching particles between the two images. The matching particles are then used to compute any translation and rotation necessary to align the two images to each other. Janus particles which are potentially too close to the edge to be analyzed are eliminated in an unbiased fashion, excluding any Janus particles whose centers are separated from the edge of the image by approximately their radius. The intensity of the pixels within the Janus particles is scaled to account for the curvature of the particle, where SEM intensity is higher at the center of the sphere and radially decreases in a well-defined pattern. The image is then thresholded using Otsu's method to determine which pixels correspond to the coated regions of the Janus particles. The centroid of the visible portion of the coated region of each particle is then calculated. The azimuthal angle φ is defined by the vector connecting the center of the Janus particle to the centroid of its coated region. The polar angle θ can be computed from the distance separating the center of the particle from the centroid of its coated region using Equation 13. However, due to pixelation, uncertainties in localization of $> \frac{1}{4}$ pixel are not uncommon; for Janus particles whose radius is 18 pixels, this would result in a reported

value of $\theta \approx 15^\circ$ for cases where the result should be $\theta = 0^\circ$. Instead, θ was calculated using Equation 11 as this was found to be less influenced by pixelation.

3. Details of MDPD Simulations

MDPD is an off-lattice, coarse-grained computational method that can efficiently simulate multi-phase, multi-component systems on the mesoscale.[2–8] In MDPD, a volume of fluid or solid is coarse-grained into individual point-mass beads; each bead represents a cluster of atoms or molecules. The dynamics of a fluidic system is dictated by the motions of beads, which are governed by Newton's equations of motion, $m\, d\mathbf{v}_i / dt = \mathbf{f}_i$. The force acting on bead *i* from neighboring beads consists of three pairwise additive terms, $\mathbf{f}_i = \sum_{j \neq i} \left(\mathbf{F}_{ij}^C + \mathbf{F}_{ij}^D + \mathbf{F}_{ij}^R \right)$. The sum runs over all beads *j* within a certain cutoff radius r_c from bead *i*.

The conservative force $\mathbf{F}_{ij}^C$ is the addition of a soft-core repulsion and an attraction, given as $\mathbf{F}_{ij}^C = A_{ij} \left(1 - r_{ij}/r_c\right)\hat{\mathbf{r}}_{ij} + B_{ij} \left(\bar{\rho}_i + \bar{\rho}_j\right)\left(1 - r_{ij}/r_d\right)\hat{\mathbf{r}}_{ij}$ with $r_{ij} = \left|\mathbf{r}_i - \mathbf{r}_j\right|$ and $\hat{\mathbf{r}}_{ij} = \left(\mathbf{r}_i - \mathbf{r}_j\right)/r_{ij}$.[9] The attraction strength A_{ij} is negative while the repulsion strength B_{ij} is positive. The two interaction parameters are given in units of $k_\mathrm{B}T/r_c$ with k_B being the Boltzmann constant and *T* is the system temperature. The many-body repulsion depends on local densities of beads, defined as $\bar{\rho}_i = \sum_{j \neq i} 15/2\pi r_d^3 \left(1 - r_{ij}/r_d\right)^2$.[9] The attraction is longer-range than the repulsion with $r_d < r_c$. This combination of repulsion and attractive was shown to produce cubic pressure-density equations of state than can exhibit a van der Waals loop, thereby permitting the liquid-vapor coexistence with a sharp interface and substantial density and viscosity contrasts.[9–11] Thus, the model explicitly captures long-range hydrodynamic interactions between colloidal particles.

The drag force $\mathbf{F}_{ij}^D = -\gamma \omega_D \left(r_{ij}\right)\left(\hat{\mathbf{r}}_{ij} \cdot \mathbf{v}_{ij}\right)\hat{\mathbf{r}}_{ij}$ and random force $\mathbf{F}_{ij}^R = \sigma \omega_R \left(r_{ij}\right)\xi_{ij}\hat{\mathbf{r}}_{ij}$ work together to impose correct dissipative dynamics at a given temperature as in the standard dissipative particle dynamics.[12–14] ω_D and ω_R are arbitrary weight functions that vanish at $r_{ij} = r_c$. $\mathbf{v}_{ij} = \mathbf{v}_i - \mathbf{v}_j$ is the relative velocity. ξ_{ij} is a Gaussian random variable with zero mean and unit variance. The value of the damping parameter γ and the noise amplitude σ are related by the fluctuation-

dissipation theorem as $\sigma^2 = 2k_B T\gamma$.[12] For simplicity, the weight functions take the forms $\omega_D(r_{ij}) = \omega_R(r_{ij})^2 = (1 - r_{ij}/r_c)^2$. These forces are also pairwise to conserve momentum for correct hydrodynamic behavior.[13,15]

The characteristic length, energy, and time scales are set as r_c, $k_B T$, and $\sqrt{mr_c^2/k_B T}$. All take the dimensionless value of 1. The equations of motion are integrated in time by the velocity-Verlet algorithm with time step $\Delta t = 0.02$. We choose $\gamma = 4.5$ to achieve rapid equilibration of the system temperature and ensure numerical stability of simulation. All simulations are performed by an in-house modification of the particle simulator LAMMPS.[16]

Colloidal particles of radii 5 and 10 are modeled in this study as frozen MDPD beads grouped into rigid bodes. The interior beads are arranged in a face-centered cubic (fcc) lattice structure with a lattice constant of 0.7 to prevent fluid beads from penetrating the particles, as shown in Fig. S1a. Surface beads are distributed uniformly on a spherical layer of the given radius based on a geodesic grid.[17–19] The combination of an interior fcc lattice and a surface geodesic gird generates an impenetrable particle a well-defined smooth surface, maintaining a high degree of symmetry.[20–22] In the simulation, we model only $\alpha = 90°$ Janus particles by distinguish all beads on one side as hydrophilic and the ones on the other side as hydrophobic. To incorporate Janus boundary roughness, the Janus plane is perturbed into a sinusoidal shape with wavelength 10 and amplitude δ_r as shown in Fig. S1b. The substrate is an amorphous layer of frozen beads with a thickness of 1. The density of substrate beads is the same as the liquid phase. Additional bounce-back boundary conditions are applied at the defined liquid-substrate interface.[20,23,24]

As in our previous work,[2] the attraction and repulsion parameters for fluid-fluid interactions are set to $A_{ff} = -40$ and $B_{ff} = 40$ with a repulsion cutoff $r_d = 0.8$. These values produce liquid and vapor phases with densities being 3.93 and 0.01, respectively. The corresponding surface tension is 2.0 and the liquid viscosity is 3.5.[2] In this model, the interface has a finite thickness of approximately 2 units in length. Evaporation is simulated by constantly removing vapor beads entering a deletion zone of thickness 5 units in length at the upper boundary of the simulation box.[2,25,26] The continuous removal of vapor beads keeps instantaneous vapor density below the

saturation vapor density at the given temperature, thereby triggering net evaporation at the liquid-vapor interface. We can model a system exposed to an ambient environment with varying vapor pressures by assigning different rates of deletion. To reduce computational cost of drying simulation, the maximum evaporation rate is imposed in this study by selecting a sufficiently high bead-removal rate, which effectively represents a system in contact with vacuum. According to previous simulation, the maximum evaporative mass flux of the particle-free interface is 2.01×10^{-3}.[2] Notably, Janus particles adsorbed at the interface will decrease the evaporation rate,[26] while the control particles immersed in the bulk have no influence. Although evaporation induces evaporative cooling effect that leads to temperature varies across the film,[25] our previous study has shown the variation is rather small (<5%) for the MDPD fluid.[2] Thus, the global thermostat as a result of the drag and random forces is applied for simplicity. In other words, we consider evaporation being isothermal in this work.

A typical simulation for probing the equilibrium particle-laden film and deposit structure contains 15 particles dispersed homogeneous in a liquid film with random orientations. The initial film dimensions are $80\times80\times15$ for $R_p=5$ particles and $160\times160\times20$ for $R_p=10$ particles, which results in a particle concentration of approximately 8% v/v and 12% v/v, respectively. The higher concentrations in the simulations are to allow the formation of large-scale assembly in computationally feasible time scales. The equilibration of the particle-laden films takes 2 million time steps to probe the assembly structure of Janus particles at the interface. Due to smaller Brownian diffusivity and capillary interactions (see Fig. 3d) of the $R_p=10$ particles, the large system is equilibrated for 8 million time steps to allow the formation of large-scale clusters. Evaporation is carried out for another 1 million time steps to obtain dried deposits.

The measurement of capillary interaction is carried out for two Janus particles adsorbed at the interface. To minimize finite size effects and improve the accuracy of force calculation, the particle pair is placed at the center of the free surface of a $80\times60\times15$ or $160\times120\times20$ film for $R_p=5$ or $R_p=10$ particles, respectively. The particle centers align with the *x* direction, consistent with the longer dimension of the simulation box. The two particles are allowed to rotate and move vertically along the *z* direction, while fixed in the *x* and *y* directions. In this manner, the inter-particle distance is well-controlled and invariant during the simulation. After

an equilibration period of 0.5 million time steps, the total force applied on each particle is calculated and its time average is taken in another 0.5 million time steps. The *x* component (along the particle-particle direction) of the force are used to compute the effective capillary force. Multiple simulations are conducted at different inter-particle distances to obtain the corresponding capillary forces.

References

(1) Jiang, S.; Yan, J.; Whitmer, J. K.; Anthony, S. M.; Luijten, E.; Granick, S. Orientationally Glassy Crystals of Janus Spheres. *Phys. Rev. Lett.* **2014**, *112* (21), 218301.

(2) Yong, X.; Qin, S.; Singler, T. J. Nanoparticle-Mediated Evaporation at Liquid–vapor Interfaces. *Extrem. Mech. Lett.* **2016**, *7*, 90–103.

(3) Yong, X. Hydrodynamic Interactions and Entanglements of Polymer Solutions in Many-Body Dissipative Particle Dynamics. *Polymers (Basel)*. **2016**, *8* (12), 426.

(4) Ghoufi, A.; Emile, J.; Malfreyt, P. Recent Advances in Many Body Dissipative Particles Dynamics Simulations of Liquid-Vapor Interfaces. *Eur. Phys. J. E* **2013**, *36* (1), 10.

(5) Chen, C.; Gao, C.; Zhuang, L.; Li, X.; Wu, P.; Dong, J.; Lu, J. A Many-Body Dissipative Particle Dynamics Study of Spontaneous Capillary Imbibition and Drainage. *Langmuir* **2010**, *26* (12), 9533–9538.

(6) Wang, Y.; Chen, S. Numerical Study on Droplet Sliding across Micropillars. *Langmuir* **2015**, *31*, 4673–4677.

(7) Zhu, Y.-L.; Liu, H.; Lu, Z.-Y. A Highly Coarse-Grained Model to Simulate Entangled Polymer Melts. *J. Chem. Phys.* **2012**, *136* (14), 144903.

(8) Stroberg, W.; Keten, S.; Liu, W. K. Hydrodynamics of Capillary Imbibition under Nanoconfinement. *Langmuir* **2012**, *28*, 14488–14495.

(9) Warren, P. B. Vapor-Liquid Coexistence in Many-Body Dissipative Particle Dynamics. *Phys. Rev. E* **2003**, *68*, 066702.

(10) Pagonabarraga, I.; Frenkel, D. Dissipative Particle Dynamics for Interacting Systems. *J. Chem. Phys.* **2001**, *115*, 5015.

(11) Trofimov, S. Y.; Nies, E. L. F.; Michels, M. A. J. Thermodynamic Consistency in Dissipative Particle Dynamics Simulations of Strongly Nonideal Liquids and Liquid Mixtures. *J. Chem. Phys.* **2002**, *117*, 9383–9394.

(12) Español, P.; Warren, P. Statistical Mechanics of Dissipative Particle Dynamics. *Europhys. Lett.* **1995**, *30*, 191–196.

(13) Hoogerbrugge, P. J.; Koelman, J. M. V. A. Simulating Microscopic Hydrodynamic Phenomena with Dissipative Particle Dynamics. *Europhys. Lett.* **1992**, *19* (3), 155–160.

(14) Groot, R. D.; Warren, P. B. Dissipative Particle Dynamics: Bridging the Gap between Atomistic and Mesoscopic Simulation. *J. Chem. Phys.* **1997**, *107* (11), 4423–4435.

(15) Español, P. Hydrodynamics from Dissipative Particle Dynamics. *Phys. Rev. E* **1995**, *52* (2), 1734–1742.

(16) Plimpton, S. Fast Parallel Algorithms for Short-Range Molecular Dynamics. *J. Comput. Phys.* **1995**, *117*, 1–19.

(17) Chen, S.; Phan-Thien, N.; Khoo, B. C.; Fan, X. J. Flow around Spheres by Dissipative Particle Dynamics. *Phys. Fluids* **2006**, *18* (10), 103605.

(18) Fan, H.; Striolo, A. Mechanistic Study of Droplets Coalescence in Pickering Emulsions. *Soft Matter*. 2012, p 9533.

(19) Yong, X. Modeling the Assembly of Polymer-Grafted Nanoparticles at Oil-Water Interfaces. *Langmuir* **2015**, *31*, 11458–11469.

(20) Liu, Y.; McFarlin, G. T.; Yong, X.; Kuksenok, O.; Balazs, A. C. Designing Composite Coatings That Provide a Dual Defense against Fouling. *Langmuir* **2015**, *31* (27), 7524–7532.

(21) Liu, Y.; Balazs, A. C. Modeling Biofilm Formation on Dynamically Reconfigurable Composite Surfaces. *Langmuir* **2018**, *34* (4), 1807–1816.

(22) Qin, S.; Yong, X. Interfacial Adsorption of PH-Responsive Polymers and Nanoparticles. *Soft Matter* **2017**, *13* (30), 5137–5149.

(23) Pan, W.; Fedosov, D. A.; Karniadakis, G. E.; Caswell, B. Hydrodynamic Interactions for Single Dissipative-Particle-Dynamics Particles and Their Clusters and Filaments. *Phys.*

Rev. E **2008**, *78* (4), 046706.

(24) Yong, X.; Kuksenok, O.; Matyjaszewski, K.; Balazs, A. C. Harnessing Interfacially-Active Nanorods to Regenerate Severed Polymer Gels. *Nano Lett.* **2013**, *13*, 6269–6274.

(25) Cheng, S.; Lechman, J. B.; Plimpton, S. J.; Grest, G. S. Evaporation of Lennard-Jones Fluids. *J. Chem. Phys.* **2011**, *134* (22), 224704.

(26) Cheng, S.; Grest, G. S. Molecular Dynamics Simulations of Evaporation-Induced Nanoparticle Assembly. *J. Chem. Phys.* **2013**, *138*, 064701.

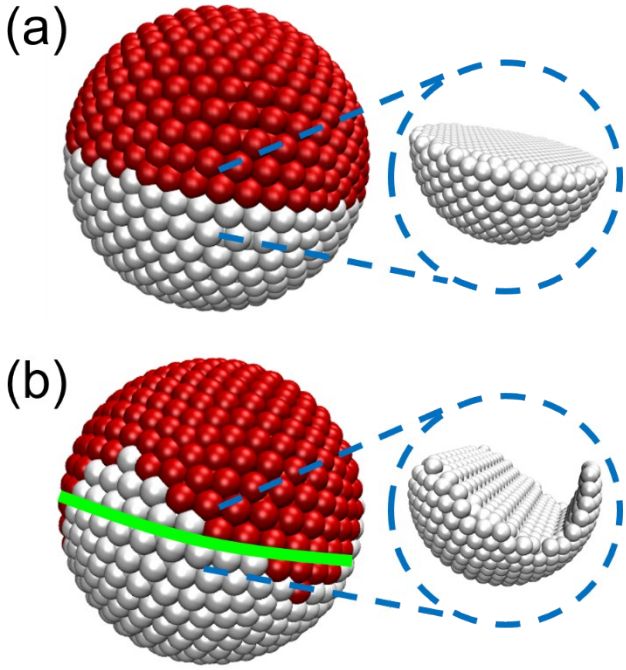

Fig. S1 Detailed structure of amphiphilic Janus particles of radius 5 with (a) smooth and (b) Janus boundaries. The amplitude of roughness $\delta_r = 3$. The insets show the Janus boundary planes. The green line in (a) is a guided line showing the position of perfect smooth Janus boundary.

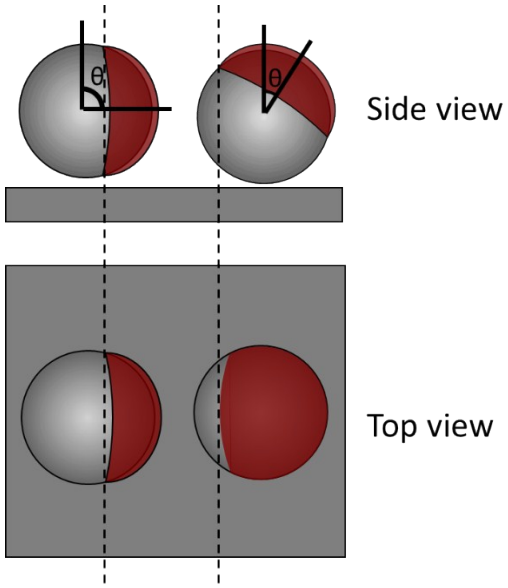

Fig. S2 Orientation determined by out-of-plane angle (θ)

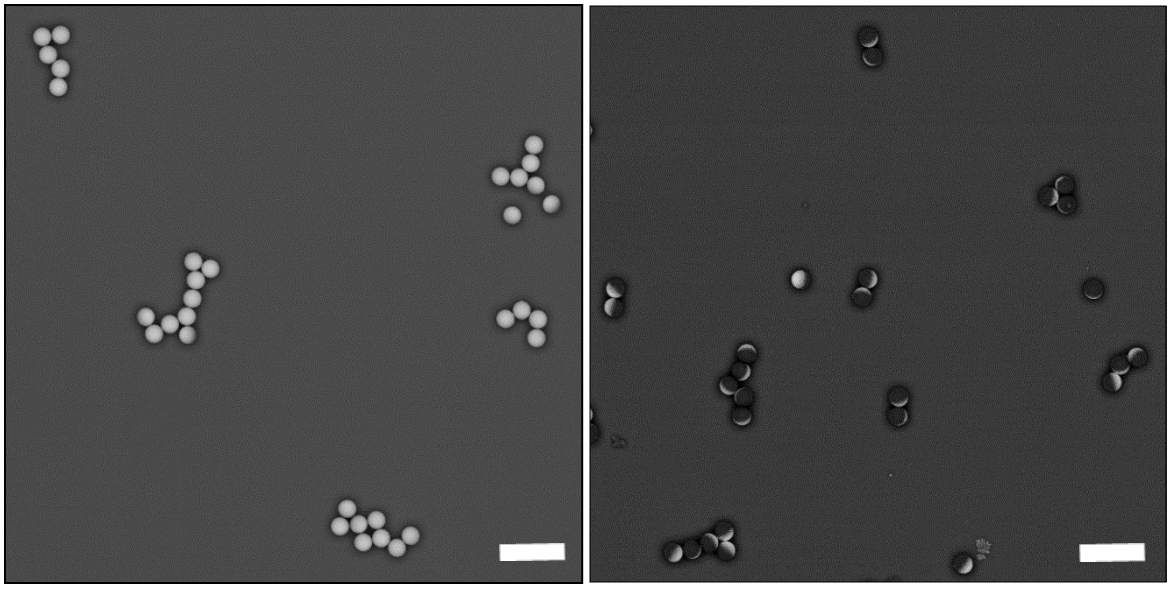

Fig. S3 Orientation and assembly of Janus particles with different surface chemistry: a) Janus particles with shorter thiol attachment JP-DDT, b) Janus particles with charged thiol JP-MHA (scale bar 10 μm).

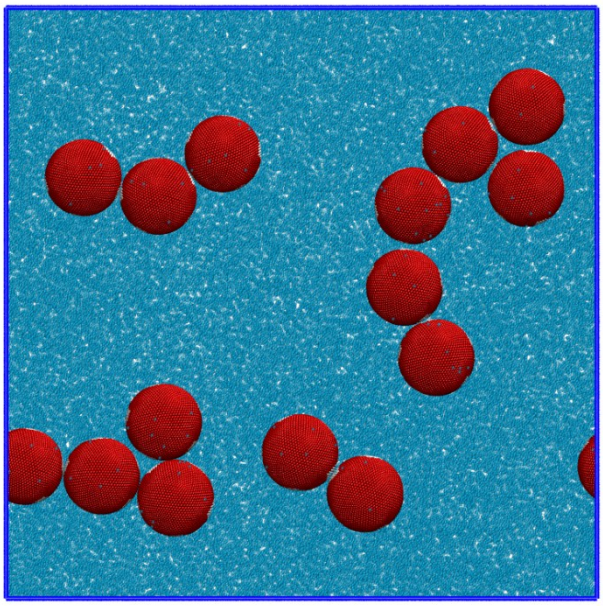

Fig. S4 Self-assembly structure of large amphiphilic Janus particles with rough Janus boundaries ($R_p = 10$ and $\delta_r = 3$) at the liquid-vapor interface.